Title

Human Induced Pluripotent Stem-Cardiac-Endothelial-Tumor-on-a-Chip to Assess Anticancer Efficacy and Cardiotoxicity

Authors

Weng, Kuo-Chan
Kurokawa, Yosuke K
Hajek, Brianna S
et al.

termis.

Tissue Engineering
& Regenerative Medicine
International Society

METHODS ARTICLE

Human Induced Pluripotent Stem-Cardiac-Endothelial-Tumor-on-a-Chip to Assess Anticancer Efficacy and Cardiotoxicity

Kuo-Chan Weng, PhD,[1] Yosuke K. Kurokawa, PhD,[1] Brianna S. Hajek, BS,[1] Jack A. Paladin, BS,[1] Venktesh S. Shirure, PhD,[2] and Steven C. George, MD, PhD[2]

Cancer remains a leading health threat in the United States, and cardiovascular drug toxicity is a primary cause to eliminate a drug from FDA approval. As a result, the demand to develop new anticancer drugs without cardiovascular toxicity is high. Human induced pluripotent stem (iPS) cell-derived tissue chips provide potentially a cost-effective preclinical drug testing platform, including potential avenues for personalized medicine. We have developed a three-dimensional microfluidic device that simultaneously cultures tumor cell spheroids with iPS-derived cardiomyocytes (iPS-CMs) and iPS-derived endothelial cells (iPS-EC). The iPS-derived cells include a GCaMP6 fluorescence reporter to allow real-time imaging to monitor intracellular calcium transients. The multiple-chambered tissue chip features electrodes for pacing of the cardiac tissue to assess cardiomyocyte function such as the maximum capture rate and conduction velocity. We measured the inhibition concentration (IC_{50}) of the anticancer drugs, Doxorubicin ($0.1 \mu M$) and Oxaliplatin ($4.2 \mu M$), on the tissue chip loaded with colon cancer cells (SW620). We simultaneously evaluated the cardiotoxicity of these anticancer drugs by assessing the drug effect on the spontaneous beat frequency and conduction velocity of iPS-derived cardiac tissue. Consistent with *in vivo* observations, Doxorubicin reduced the spontaneous beating rate and maximum capture rate at or near the IC_{50} (0.04 and $0.22 \mu M$, respectively), whereas the toxicity of Oxaliplatin was only observed at concentrations beyond the IC_{50} (33 and $9.9 \mu M$, respectively). Our platform demonstrates the feasibility to simultaneously assess cardiac toxicity and antitumor effects of drugs and could be used to enhance personalized drug testing safety and efficacy.

Keywords: organ-on-a-chip, iPS-cardiomyocyte, iPS-endothelial cell, cancer drug testing

Impact Statement

Drug development using murine models for preclinical testing is no longer adequate nor acceptable both financially for the pharmaceutical industry as well as for generalized or personalized assessment of safety and efficacy. Innovative solutions using human cells and tissues provide exciting new opportunities. In this study, we report on the creation of a 3D microfluidic device that simultaneously cultures human tumor cell spheroids with cardiomyocytes and endothelial cells derived from the same induced pluripotent stem cell line. The platform provides the opportunity to assess efficacy of anticancer agents while simultaneously screening for potential cardiovascular toxicity in a format conducive for personalized medicine.

Introduction

CANCER AND HEART DISEASE are, by far, the two leading causes of mortality in the United States. There remains a need for continued innovation in the development of new therapeutic options, including pharmaceutics. While two-dimensional (2D) cell culture systems remain the mainstay due to simplicity, reproducibility, and affordability, these systems do not capture the rich cell–cell and cell–matrix interactions of the three-dimensional (3D) *in vivo* tissue microenvironment that has been shown to be crucial to predict drug response.[1] Moreover, while there is not normally an obvious connection (e.g., cardiac tumors) between the diseases, it is well-documented that several prominent chemotherapeutic

[1]Department of Biomedical Engineering, Washington University in St. Louis, St. Louis, Missouri.
[2]Department of Biomedical Engineering, University of California, Davis, Davis, California.

agents (e.g., Doxorubicin, cyclophosphamide) have detrimental effects on cardiac function,[2,3] and both cardiomyocytes and many tumor cells share expression of prosurvival proteins and tyrosine kinases, the latter of which is a promising new target for a family of anticancer agents.[4]

Although the frequency of cardiac side effects can be small, the consequences are severe and include diffuse cardiomyopathy and arrhythmias, which severely compromise quality of life, have limited therapeutic options, and can result in sudden cardiac death.[5] Our ability to predict cardiac side effects from anticancer drugs is limited by a poor understanding of the underlying mechanisms, animal models that do not replicate the human condition and have limited throughput to detect rare events, and simple 2D *in vitro* culture systems. The development of advanced 3D human micro-organ systems that include tumor, cardiac muscle, and/or the vasculature in a flexible and modular design could provide: (1) a major advance in anticancer drug discovery while minimizing cardiac side effects; (2) a model of perfused cardiac muscle for cardiovascular drug discovery; and (3) the flexibility to recombine these micro-organs, or additional micro-organs (e.g., liver, pancreas, bone marrow) impacted by chemotherapeutics.

To replicate the complex 3D arrangement of cells and extracellular matrix, new human micro-physiological systems must be developed that include a vascular supply. The vasculature not only provides the necessary convective transport of nutrients and waste in 3D culture, it also couples and integrates the response of multiple organ systems. *In vivo*, drugs or nutrients permeate through the vascular wall, where they are distributed by convective and diffusive transport throughout a tissue. These features are clearly absent in 2D or simpler 3D models. Recent studies have addressed this issue by developing tumor-on-a-chip systems with a vascular supply.[6] Interestingly, drug responses of tumor-on-a-chip systems with and without vasculature have been significantly different.[7] Comparatively, development of vascularized heart-on-a-chip systems has been slow because the source of human-derived cells is limited and developing a 3D system with noninvasive and easily measurable endpoints is challenging. As a result, an integrated platform of human cardiac, vascular, and tumor tissues has not been developed and thus our understanding of basic features, such as the simultaneous impact of drugs on the electrophysiological properties of cardiomyocytes and tumor viability has not been explored.

The objective of this study was to develop an integrated platform to simultaneously analyze the anticancer and potential cardiotoxicity of chemotherapeutics. We utilize induced pluripotent stem cell-derived cardiomyocytes (iPS-CM) and endothelial cells (iPS-EC) from the same parental iPS cell line and integrate these tissues with human tumors on a single platform. We analyze the effect of drugs on growth of tumor and function of cardiomyocytes using noninvasive and nondestructive methods so the platform can be used for repeated measurements to potentially monitor long-term drug effects continuously. Our data demonstrate that this technology could be used to improve the efficiency and thus lower the cost of preclinical drug discovery by simultaneously determining a drug's anticancer and cardiotoxicity potential.

Materials and Methods

Microfluidic device design and fabrication

Our device design is influenced by the *in vivo* observations that a capillary exists near every cell in the human body. We scaled our device to create tissues within a physiologic distance from capillaries ($<250\,\mu m$).[8] The volume of tissue fed by a capillary of $1\,mm^2$ surface area is in the range between 0 and $6\,mm^3$ (volume to surface ratio [*V/S*] range between 0 and 6 mm). We used this feature to scale the device design. The *V/S* ratio in our device is controlled by the number of pores where the endothelial cells attach. We chose the density of pores to be 3.2 per millimeter, which yields *V/S* close to 2.5 mm (a range similar to that of *in vivo* tissues).[9]

The multichamber microfluidic tissue chip was fabricated using soft lithography and replica molding techniques described previously by our group and others.[10] The microfluidic devices were fabricated using polydimethylsiloxane (PDMS, Sylgard 184; Dow Corning) and assembled together on glass slides with patterned gold electrodes by plasma bonding to allow electrical stimulation for cardiac tissue (Fig. 1a). We designed three pairs of electrodes on a single gold-coated glass slide (TA134; Evaporated Metal Films Corporation) such that each pair of electrodes could electrically stimulate a separate iPS-derived cardiac tissue (Fig. 1b, c) to measure endpoints, including conduction velocity and maximum capture rate. The tissue chips were autoclaved and stored until tissue loading. Alligator clips were used to connect the electrode-patterned slides to the signal generator MyoPacer (IonOptix) to stimulate the cardiac tissue at the specified frequencies under 5 V. The system was supported by gravity-driven static flow from the central chamber (high pressure) and side fluidic lines (low pressure) (Fig. 1b).

Cell culture

The iPS cells were maintained with E8 medium (A1517001; Thermo Fisher Scientific) and passaged every 4 days. The iPS cells were integrated with a GCaMP6 reporter in the AAVS1 safe harbor locus to monitor intracellular calcium transients as previously described.[11] The creation of cardiomyocytes from iPS cells (iPS-CM) was achieved by modulating WNT signaling as previously described.[12] In short, $6\,\mu M$ of CHIR99021 (C-6556; LC Laboratories) was supplemented through day 0 to 2 to activate WNT signaling and $5\,\mu M$ of IWP2 (3553; Tocris) was supplemented through day 3 to 5 to inhibit WNT signaling. The spontaneously beating sheets of cells were observed at day 7. The iPS-CMs were further purified between day 13 to 21 by glucose deprivation and the medium used was 4 mM of sodium DL-lactate solution (L4263; Sigma) and 25 mM of HEPES (15630080; Thermo Fisher Scientific) in glucose-free RPMI 1640 medium (11879020; Thermo Fisher Scientific).[13] Purified iPS-CMs were harvested for tissue chip loading between day 30 and 45. We also used a CDH5-mcherry stable clone of the WTC-11 iPS cell to allow real-time imaging of endothelial cells as previously described.[14] The differentiation of the iPS cells into endothelial cells (iPS-EC) was performed by modulating TGF-β signaling as previously described and purified by magnetic sorting of

CD31-positive cells.[14] The iPS-ECs were cryopreserved at day 6 and were thawed and expanded for another 5 days before tissue chip loading. We chose colon adenocarcinoma cell line SW620 as this cancer cell line is commonly used to model colon cancer, and the colon is routinely treated for colon cancer. Furthermore, the SW620 cells form tumor spheroids in the device, which are simple to quantify growth using fluorescent imaging. The SW620 cell was lentivirally transduced with a constitutively expressing GFP reporter and were cultured with DMEM supplemented with 10% (v/v) of fetal bovine serum.

Tissue chip loading

We used the blunt end of a needle to punch the PDMS device to create the inlets for reservoirs of media and to load the tissue chambers. Pipette tips served as media reservoirs and the tissue chips were supported by gravity-driven flow by adjusting the differences of liquid level in the pipette tips between the central chamber and side fluidic lines (Fig. 1a, d). The central chamber was loaded with iPS-EC and allowed to form a confluent monolayer (Fig. 1e, f and Supplementary Figs. S1–S3). The central endothelial-lined chamber was then supplied with media (with or without drug) at a high pressure (high medium level—100 μL, 2 cm in height) to drive fluid, nutrients, and drugs from the central chamber out to both of the adjacent chambers simultaneously. The bottom chamber was loaded with iPS-CM in a fibrin gel to form cardiac tissue (Fig. 1g and Supplementary Fig. S4) and the top chamber was loaded with tumor cells in a fibrin gel to form tumor spheroids (Fig. 1h, i). The side fluidic lines were supplied with lower medium levels (10 μL, 0.2 cm in height) relative to the central chamber (Fig. 1b). In this fashion, fluid, nutrients, and drugs initially flow down the central chamber, but the pressure driving force down the central chamber quickly approaches 0. At this point, the system was maintained by the gravity-driven flow from the liquid level differences between central chamber (high-pressure end) and the side fluidic lines (low-pressure end).

To load the tissue chip, we first delivered the tumor cells and iPS-CM within a fibrin gel on the side chambers (tumor on the top and iPS-CM on the bottom chamber). We mixed tumor cells (2×10^5/mL) and iPS-CMs (1×10^8/mL) with a fibrinogen (10 μg/mL)-thrombin solution and loaded the mixture into the side chambers before the fibrin gel polymerized. Once the fibrin gels were formed, we coated the central chamber with fibronectin (50 μg/mL) for 15 min and then loaded iPS-ECs (3×10^7/mL) into the central chamber. The cells were incubated for at least 1 h without disturbing to allow the iPS-ECs to form a confluent monolayer in the central chamber. The excess or unattached iPS-ECs were removed after feeding and medium change. We maintained the device with EGM2 medium (CC-3162; Lonza), which was replaced daily until drug studies and the drug solution were also delivered to the central chamber.

Finite element simulations

We created a computational model of mass and momentum transport using COMSOL Multiphysics® 5.2a (COMSOL, Inc., Burlington, MA) combined with the CAD model of the device. To simulate the flow throughout the device, a 2D steady-state solution of the incompressible Navier–Stokes equations was calculated using the flow through porous media module in COMSOL. The pressure at the loading ports of the central line were varied and set at 24.5, 18.5, or 12 mm, and the pressure at the cell loading ports and the side fluidic lines were set at 0 mm. These pressure heads corresponded to the differential pressures created in experiments. A matrix with 0.99 porosity was assumed to fill the tumor and cardiac chamber. The hydraulic conductivity of the tissues was varied between 1×10^{-12} and 1×10^{-17} m^2 and the flow rate of fluid exiting the fluidic lines was computed for each hydraulic conductivity. For this, the velocity found by COMSOL was integrated over the cross-sectional area of pores between the tissue chamber and the fluidic lines.

The unsteady state of transport in diluted species module coupled with flow through porous media module was also used

FIG. 1. Three-chamber microfluidic device design. **(a)** Schematic diagram of the three-chamber microfluidic tissue chip design. The microfluidic device is 100 μm in height and was maintained by gravity-driven flow from the differences of the liquid level (Δh) between the central chamber and side fluidic lines. The medium and drugs were delivered from the central chamber (high pressure, *red*) to the side fluidic lines (low pressure, *yellow*). Tumor and iPS-CM were loaded in the side chamber with fibrin gel (*green*) and iPS-EC were loaded in the central chamber to form a continuous monolayer (*red*). The glass slide was patterned with gold electrodes and plasma bonded with the PDMS microfluidic device. **(b)** Detailed schematic diagram of three-chamber tissue chip. The *arrows* (*blue*) demonstrate the fluidic flow from the central chamber to the side fluidic line through the pores (30 μm wide). **(c)** Three PDMS microfluidic devices were plasma bonded on a single gold electrode-patterned glass slide. **(d)** The fluorescence image demonstrates the three-chamber tissue chip loaded with GFP-SW620 tumor spheroid (*top*, *green*), GCaMP6-iPS-CM (*bottom*, *green*) and CDH5-mCherry-iPS-EC (*center*, *red*). The *black lines* on the left are the gold electrodes, and the *red color* in the bottom chamber is background (not endothelial cells, see Supplementary Fig. S1). **(e)** Confocal image shows three-dimensional structure of three-chamber tissue chip. The tissue chip compartments were labeled with CD31 (iPS-EC, *yellow*), cardiac troponin TNNT2 (iPS-CM, *green*), and the nuclei were counterstained with DAPI (*blue*). The X' and Y' section plane (120 μm in height) shows the iPS-EC form a lumen in the central chamber (*arrow*). The Y' focal plane also shows the three-dimensional structure of both tumor spheroid on the top chamber and the cardiac tissue on the bottom chamber. The scale bar is 200 μm. **(f)** Fluorescence image of the central chamber in the tissue chip labeled with CD31 (*yellow*) and DAPI (*blue*) demonstrates the junctions between the endothelial cells. The scale bar is 200 μm. **(g)** Fluorescence images of the bottom chamber in the tissue chip labeled with cardiac troponin TNNT2 (*green*) shows the structure of the cardiac tissue. The scale bar is 100 μm. **(h)** Confocal image shows the tissue chip counterstained with DAPI (*cyan*). The scale bar is 200 μm. **(i)** The Z-stack (70 μm in height) of the confocal image of **(h)** shows the three-dimensional structure of tumor spheroid. The scale bar is 200 μm. iPS-CM, iPS-derived cardiomyocytes; iPS-EC, iPS-derived endothelial cells; PDMS, polydimethylsiloxane.

to model the drug transport. Initially, the central chamber was filled with the drug while the side chambers had no drug. The partition coefficient of drug in endothelium was assumed to be 1. The concentration profiles were calculated at various time points.

Characterization of mass transport in microfluidic device

To determine the permeability of endothelial cells lining the cardiac and the tumor tissues, we perfused TRITC-labeled 70 kD dextran through the central chamber of the device (Fig. 2a, b). The devices were placed on a motorized inverted microscope (IX83; Olympus, Tokyo, Japan) connected to computers with MetaMorph Advanced (version 7.8.2.0) and equipped with an environmental control chamber to maintain temperature at 37°C and 5% CO_2 to acquire the real-time fluorescence signal (6 frames per minute, fps). Image analysis was performed using ImageJ 1.47V. First, a rate of change of fluorescent intensity was determined for a fibrin-only tissue that had a low number (200 cells/μL) of tumor cells and lacked
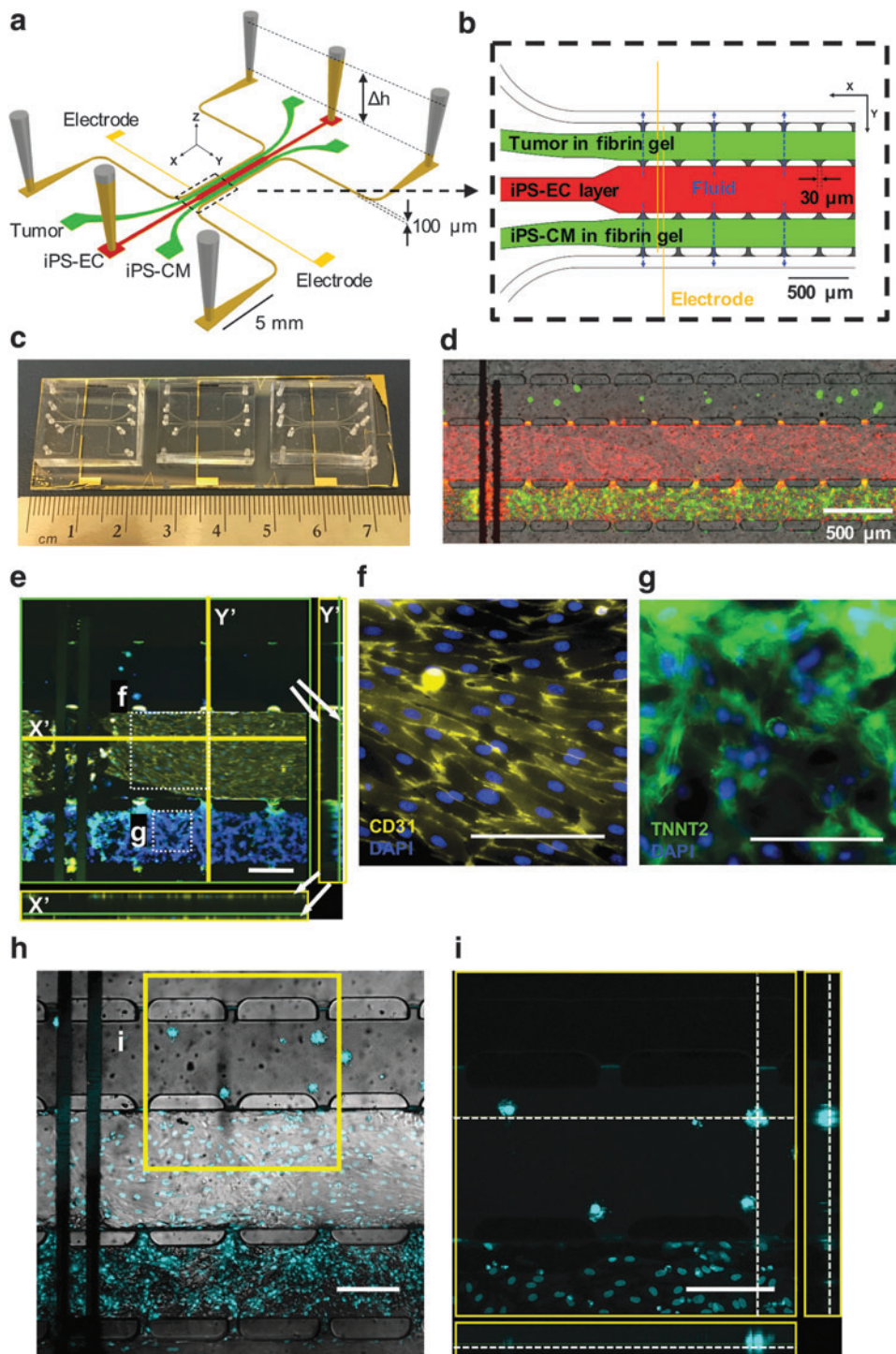
FIG. 2. Transport rates of endothelial coated chamber. (a, b) TRITC-70 kD-Dextran (*red*) solution was introduced to the tissue chip from the central chamber in the (a) presence or (b) absence of the iPS-EC endothelial layer (c) The devices were maintained using various ΔP across the tissues. The volume of media leaking from the tissue was collected for 6 h to calculate the flow rate. The COMSOL model was used to fit the experimentally measured flow rates to the hydraulic conductivities of the tissues. The K value with minimum root mean square error with respect to the experimental measurement was found for the tumor and cardiac tissues and plotted in the graph. (d) The pressure and streamline profile of the device for $\Delta P = 185$ Pa used to perform the drug studies.
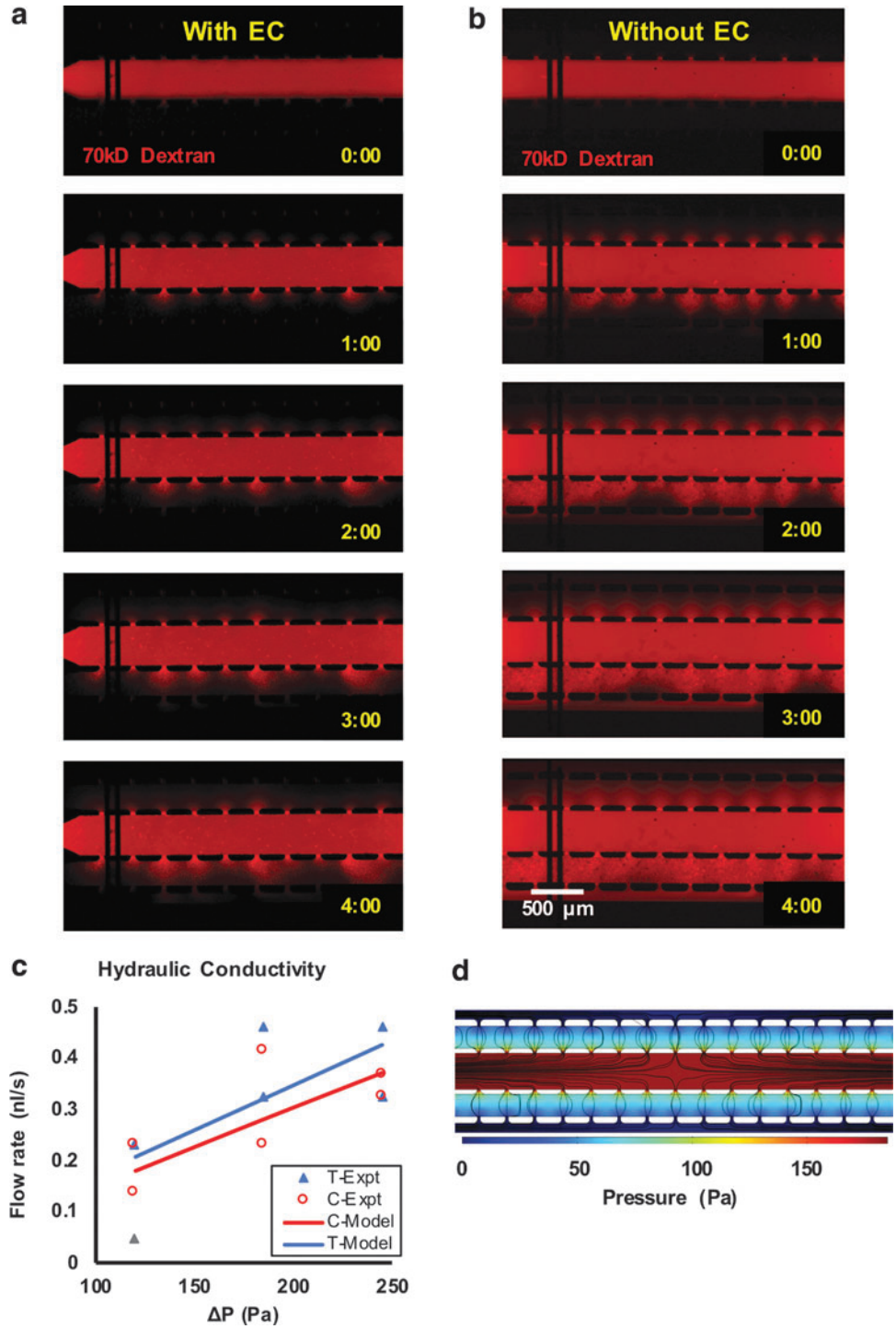
endothelial cell coating. The relative permeability of the endothelial cells was defined as the ratio of the rate of change in intensity in a tissue to that in the control tissue as follows,

$$P_r = \frac{d\left(\frac{I}{I_o}\right)}{dt} / \left(\frac{d\left(\frac{I}{I_o}\right)}{dt}\right)_c \qquad (1)$$

where P_r is relative permeability, I_o is fluorescent intensity in the cell-coated channel, $\frac{d\left(\frac{I}{I_o}\right)}{dt}$ is the normalized change in intensity with respect to time and the subscript "c" indicates control tissue.

To estimate the hydraulic conductivity (K_H) of the tissues, we used a semiempirical approach. We created cardiac or tumor devices coated with an endothelial cell layer and experimentally measured the volumetric flow rate of fluid exiting the cardiac and tumor compartments for 6 h over a series of pressure gradients created across the tissues (Fig. 2c). We then used the mathematical model of transport (COMSOL) to estimate the K_H by minimizing the error between experimentally measured and calculated flow rates.

TABLE 1. POTENTIAL DRUG LOSS DUE TO ABSORPTION INTO THE POLYDIMETHYLSILOXANE MICROFLUIDIC DEVICE

	MW	D_p (m^2/s)	LogK	Drug loss (%)
Doxorubicin	580.0	1.7E-15	1.3	0.6
Oxaliplatin	397.3	4.5E-15	−0.5	0.0

Drug losses were calculated based on the molecular properties, including MW, D_p, and K over the experiment period (48 h).[15]

D_p, diffusion coefficient; K, partition coefficient; MW, molecular weight.

Drug absorption and exposure

The potential drug loss into PDMS was considered based on the molecular properties of the drugs (Table 1). To estimate the maximum possible loss, we assumed that the drug concentration in the central chamber was steady and did not decrease appreciably along the length of the channel from inlet to outlet, and the PDMS surface was without an EC coating. We observed that the levels in the inlet and outlet reservoirs tend to equilibrate within the first hour. Therefore, the flow through the channel was assumed as 0. We adapted our previously published mathematical model for the no-flow case as follows. The flux of drug at the PDMS wall was used to calculate the drug loss from the solution as a percentage of the drug delivered to the device:

$$\text{Drug loss } (\%) = 100 \, \frac{K}{V} \sqrt{\frac{D_p}{\pi t}} S * t \qquad (2)$$

where, K is PDMS–Water partition coefficient of the drug and can be approximated by the octanol–water partition coefficient, D_p is diffusion coefficient of drug (m^2/s) in PDMS, and can be estimated using molecular weight as previously described, S is surface area (9.5 mm^2) of the drug channel exposed to PDMS, t is time (s) of drug exposure, and V is the volume of drug added to the device volume (m^3) of channel.[15]

We examined the effects of two anticancer drugs, one with known cardiotoxicity (Doxorubicin, D1515; Sigma-Aldrich) and one without any known cardiac side effects (Oxaliplatin, O-711; LC Laboratories). Doxorubicin was reconstituted in water at 10 mM and Oxaliplatin was reconstituted in DMSO at 10 mM and stored in −80°C. The drugs were diluted to the desired concentration in EGM2 culture medium and delivered to the tissue chip from the central chamber. The vehicles (water for Doxorubicin and DMSO for Oxaliplatin, respectively) were used in each drug experiment as the control group to compare the drug effect in experimental groups. The medium delivered to the tissue chip was replaced every 24 h and the drug effects were assessed at 48 h. At least three independent tissue chips were included in each drug concentration to assess the drug effects on tumor growth and cardiac function. Depending on the tissue chip loading condition, each tumor chamber from different tissue chips consisted of different amounts of tumor spheroids, ranging from 5 to 20, and all spheroids were included to quantify the growth area. We included seven concentrations of each drug to determine the inhibition concentration (IC$_{50}$) of tumor growth. In some conditions, the cardiac function of the tissue chip failed (e.g., cardiac tissue not paced so that maximum capture rate was not defined) and thus those conditions were excluded from the IC$_{50}$ curve.

Brightfield, fluorescence, and immunofluorescence imaging

The brightfield and fluorescence images were acquired using an Olympus IX83 Microscope System. The stream acquisition of the GCaMP6 signal was carried out at 100 fps and images were interpreted by a custom-developed MATLAB code to determine spontaneous beating rate, maximum capture rate, and conduction velocity. The immunofluorescence staining of the tissue chip was carried out by flowing the reagents from the central chamber to the side chambers. After drug testing and imaging acquisition, the devices were washed by PBS once and fixed with 4% (v/v) paraformaldehyde for 1 h. The tissue chips were stained by adding primary antibody followed by secondary antibody and nuclei counterstain was conducted by DAPI solution (1 μg/mL). The negative control staining was conducted with secondary antibodies alone (Supplementary Fig. S5). The antibodies used for immunofluorescence staining were CD31 (M082301; Dako), TNNT2 (ab45932; Abcam), Alexa Fluor 488 goat anti-rabbit IgG antibody (A11008; Invitrogen), and Alexa Fluor 555 goat anti-mouse IgG antibody (A21422; Invitrogen).

Quantification of the growth area of tumor spheroids

To assess the growths and drug effects of tumor spheroids, we quantified the total growth area of the tumor spheroids in each tissue chip by taking the multiple color images of tissue chips and calculating the area of each spheroid. The brightfield channel was used to quantify the growth area (Supplementary Fig. S6). The green fluorescence channel was only used to better locate the viable tumor spheroids to prevent overexposure. The tumor chamber consisted different amounts of tumor spheroids (range from 5 to 20) in each tissue chip. All spheroids in the tumor chamber were included to quantify the growth area using ImageJ. To quantify the growth of tumor spheroids, the total growth area of the tissue chips at 48 h was first normalized with the area at their 0 h. Then, to assess the drug effects on tumor growth, the total growth area in the tissue chips treated with drugs was compared with the tissue chips treated with vehicle controls (water for Doxorubicin and DMSO for Oxaliplatin). The fold change at each drug concentration (compared with the vehicle control) was plotted and the four-parameter logistic model was fit to determine the IC$_{50}$ of each drug using Prism 7.

Cardiac function analysis

The spontaneous beating rate was determined by the *findpeaks* function in a custom-developed MATLAB code at the 0 Hz interval. The maximum capture rate was determined by the highest frequency that the cardiac tissues could be paced using the following frequencies (1.0, 2.0, 2.4, 2.8, or 3.2 Hz). The conduction velocity was determined by calculating the time difference between the peak of GCaMP6 intensity between two given regions in the cardiac chamber of the tissue

chip. We choose the region on the left end and the region on the right end to define the distance (Δd). We stimulated the cardiac tissue from one end using MyoPacer and then recorded the fluorescence intensity as a function of time. The conduction velocity (v) is determined by dividing the distance traveled by the fluorescent wave by the period of time ($v = \Delta d / \Delta t$).

Statistical analysis

At least three biological replicates were performed in all experiments and data are reported as mean $\pm$ S.E.M. Graph-Pad Prism 7 was used to perform the statistical analysis. Unpaired t-test and one-way analysis of variance was used to compare columns and the p-values <0.05 were considered statistically significant. The data were analyzed and graphed using Microsoft Excel and GraphPad Prism 7.

Results

iPS-derived endothelial layer provides physiological barrier

After loading, the tissue chips were allowed to stabilize for two days. During this period, the iPS-EC formed a confluent monolayer over the entire surface of the central chamber (Fig. 1e). Confocal imaging demonstrated continuous coverage of the central chamber and intact junctional complexes (Fig. 1f and Supplementary Figs. S2 and S3). The iPS-CM form a 3D cardiac-like tissue in the bottom compartment (Fig. 1e), and the sarcomere structure can be seen by visualizing cardiac troponin (Fig. 1g and Supplementary Fig. S4). Three-dimensional tumor spheroids can be seen in the top compartment (Fig. 1h, i).

To assess barrier function of the iPS-EC layer to large molecules, we introduced TRITC-conjugated 70-kD dextran through the central chamber and measured the change in fluorescence intensity over time (Fig. 2a, b) in the adjacent chambers. The endothelial monolayer lining the central chamber provided a barrier to dextran transport. More specifically, the permeabilities of the cardiac and tumor tissues in the presence of the iPS-EC lining were 74% and 25%, respectively, compared with the permeability in the absence of the endothelium.

Mainstream chemotherapeutic drugs are small molecules with molecular weights <1 kD. The resistance to the transport of drug molecules is generally lower than the resistance to large molecules. To characterize the tissue for transport of small molecules, we analyzed water transport by estimating the hydraulic conductivity, K_H, of the tissue. We experimentally measured the flow exiting the side microfluidic lines at various pressure gradients created across the tissues (Fig. 2c). The COMSOL model (Fig. 2d) shows the pressure and streamline distributions. For tumor and cardiac tissues, K_H was determined by minimizing the root mean square error between the model and experimental data. The value for tumor and cardiac tissue were 1×10^{-15} and 0.8×10^{-15}, respectively. The flows calculated using these values of K_H generally fall in the range of experimentally measured flows (0.39 ± 0.069 and 0.32 ± 0.093 nL/s for tumor and cardiac chamber, respectively) (Fig. 2c). To determine whether the small difference in K_H impacts the time for drugs to reach steady state in either of the tissue chambers, we calculated

the concentration profiles for a hypothetical drug molecule with partition coefficient of 1. The time required to reach >90% of steady state for either tissue was <80 min (Supplementary Fig. S7). These data indicate that the rate of transport of the drug is essentially identical in the cardiac and tumor chamber.

We also considered drug absorption from the PDMS and calculated the potential loss of each drug used in this study based on their molecular weights, hydrophobicity, and other chemical properties using Equation (2) (Table 1).[16] Drug loss for Oxaliplatin and Doxorubicin was estimated to be <1% per day (24 h) of treatment.

Anticancer drugs inhibit colon tumor cell growth

We quantified the growth of tumor spheroids with Doxorubicin treatment of 24, 48, and 72 h and found a statistically significant effect at 48 h (Supplementary Fig. S8). Therefore, we determined the dose–response of the chemotherapeutic drugs between 0 and 48 h. Under vehicle (DMSO) control groups, the tumor cells grew and formed spheroids after 48 h (Fig. 3a). When we treated the tissue chip with anticancer drugs, Doxorubicin and Oxaliplatin, the tumor cell growth was limited as the drug concentration progressively increased (Fig. 3a).

We normalized the growth area at 48 to 0 h for each tissue and at each concentration, and then normalized each value to the corresponding vehicle control group (Supplementary Fig. S6). The IC$_{50}$ of Doxorubicin and Oxaliplatin (0.11 and 4.27 μM, respectively) (Fig. 3b, c) were determined from the dose–response curve.

Cardiotoxicity of anticancer drugs

Cardiomyocyte function was assessed by quantifying the spontaneous beat rate, maximum capture rate, and conduction velocity using the transient intracellular calcium concentration (GCaMP6 fluorescent signal). At 0 and 48 h, we paced the cardiac tissue through the patterned gold electrodes at 5 V with a range of frequencies (0, 1, 2, 2.4, 2.8, to 3.2 Hz) (Fig. 4a). These stream images were analyzed using a custom-developed MATLAB code to determine the spontaneous beating rate (at 0 Hz) and maximum capture rate (highest frequency that the cardiac tissue could be paced).

The spontaneous beating rate of the control cardiac tissues was 49 ± 3.4 beats per minute (bpm) at 0 h, which decreased to 30 ± 1.7 bpm at 48 h (Supplementary Fig. S9). At 48 h, Doxorubicin had no effect on the beating rate at 0.1 μM (36 ± 6 bpm) but reduced the beating rate at 1 μM (13 ± 12 bpm) and completely eliminated spontaneous beating at 10 μM (Fig. 4b). At 48 h, the beating rates were not impacted when treated with Oxaliplatin at 0.1 μM (42 ± 18 bpm) and 3 μM (43 ± 22 bpm) but decreased to 25 ± 14 bpm at 33 μM. Oxaliplatin completely eliminated spontaneous beating at 50 μM (Fig. 4c). The IC$_{50}$ for spontaneous beating rate was 0.04 and 33 μM for Doxorubicin and Oxaliplatin, respectively.

The maximum capture rate of the cardiac tissues was more difficult to measure than spontaneous beat rate; hence, we were not able to measure this index in as many tissues or at as many drug concentrations. Nonetheless, the trends for IC$_{50}$ were similar compared with spontaneous beat rate. The IC$_{50}$ for maximum capture rate was 0.2 and 10 μM, respectively, for Doxorubicin and Oxaliplatin (Fig. 4d, e).
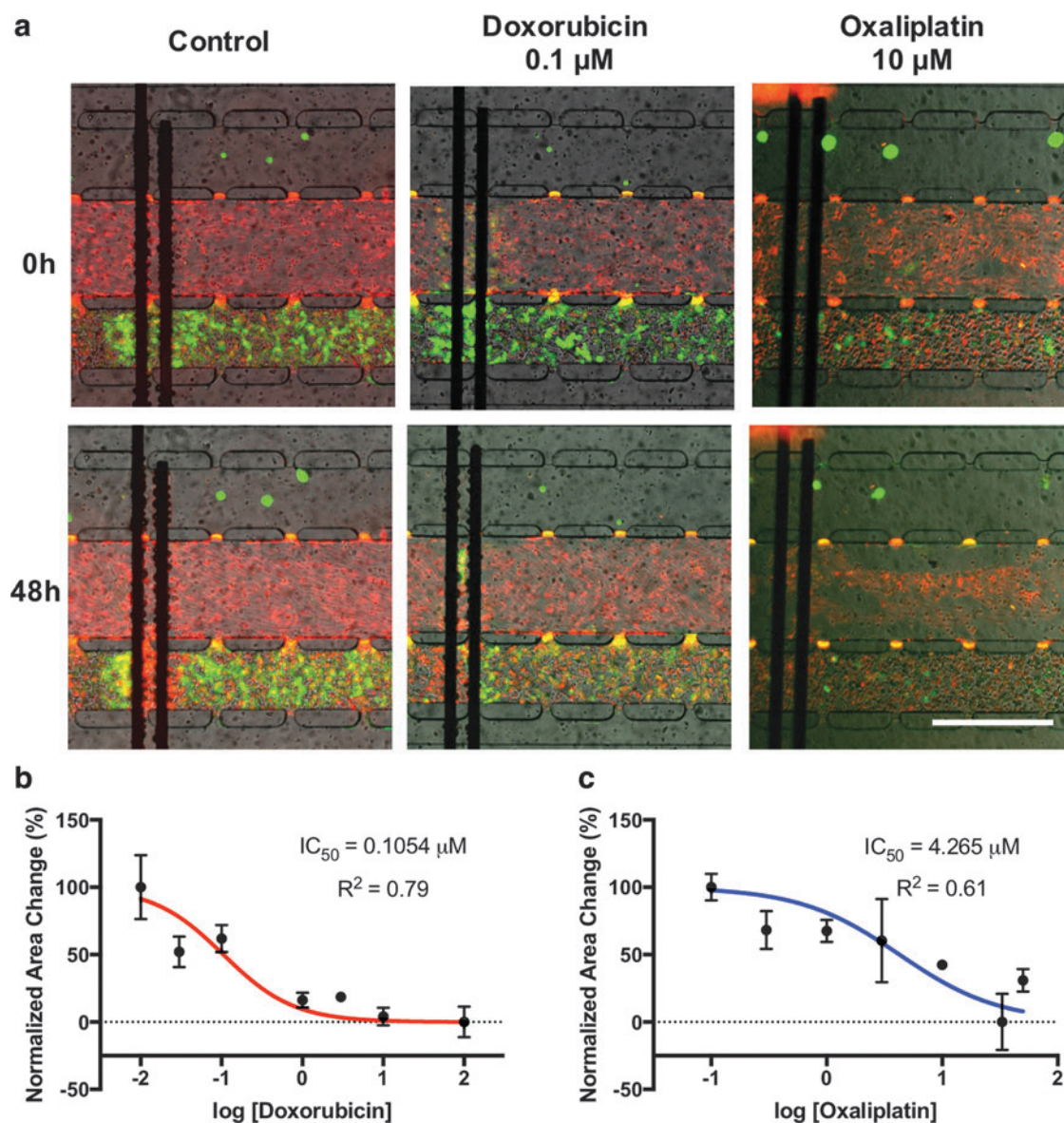
FIG. 3. Tumor growth inhibition by anticancer drugs. **(a)** Fluorescence images of the tissue chip before and 48 h after drug treatment (0.1 and 10 μM). The top chambers were loaded with GFP-SW620 tumor spheroids (*green*), the central chambers were loaded with CDH5-mCherry-iPS-EC (*red*), and the bottom chambers were loaded with GCaMP6-iPS-CM (*green*). The scale bar is 500 μm. **(b, c)** The dose–response of the tumor growth area to the anticancer drugs **(b)** Doxorubicin and **(c)** Oxaliplatin. The tumor growth represents the area of tumor after 48 h of drug exposure normalized by the area at time 0, and then normalized by the value at 0 concentration. All tumor spheroids (between 5 and 20) in the tumor chamber of each tissue chip were included and three independent tissue chips were used to calculate the area change. The area change of each drug concentration was normalized to its own control (water and DMSO for Doxorubicin and Oxaliplatin, respectively) condition and the plot was presented as mean ± S.E.M. The IC_{50} curves were fit with four-parameter logistic model. IC_{50}, inhibition concentration.

We measured the conduction velocity of cardiac tissue by electrically stimulating the cardiac tissue at the left-hand side of the tissue using the gold electrodes. The GCaMP6 intensity was captured using stream acquisition at 100 fps (Fig. 5a). We chose two regions, one from the left end and one from the right end to determine Δd. We plotted the GCaMP6 intensities of these two regions over time and used custom-developed MATLAB code to determine the time of peak (t) (Fig. 5b). The conduction velocity was determined by simply dividing the distance (Δd) by the time difference of peak (Δt). The conduction velocity of the cardiac tissue at 0 h was 2.1 ± 0.3 cm/s and increased to 4.6 ± 2.0 cm/s at 48 h (Fig. 5c).

Discussion

In this study, we developed a three-chamber microfluidic tissue chip that simultaneously supports three tissues: tumor spheroids, an endothelium, and cardiomyocytes. The endothelial cells and cardiomyocytes in the platform are derived
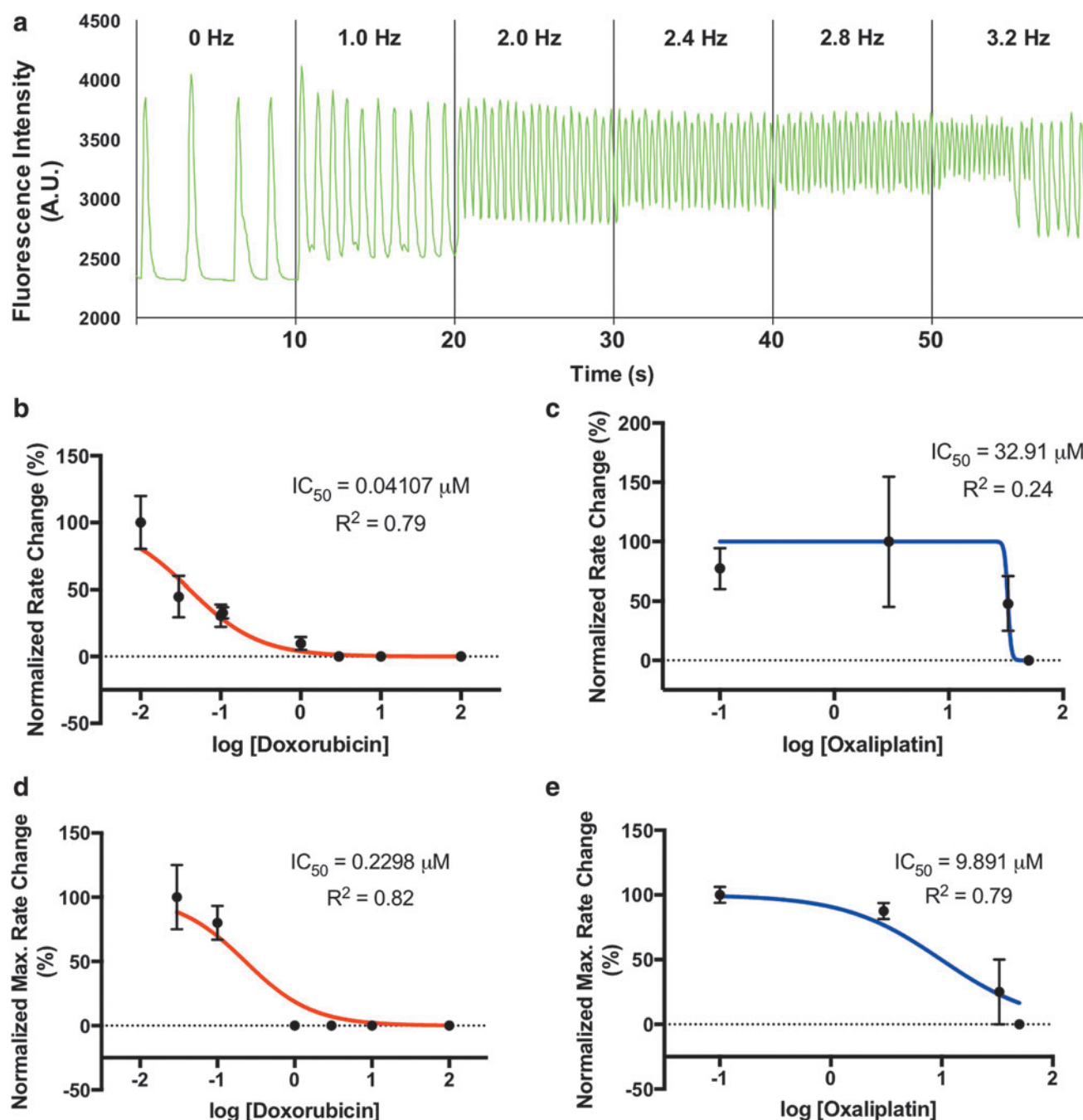
FIG. 4. Anticancer drug effects on cardiac tissue. **(a)** The fluorescence (GCaMP6) intensity of the cardiac tissue as a function of time during pacing at different frequencies. The device was electrically stimulated at the indicated frequencies through the patterned electrodes. **(b, c)** The dose–response of spontaneous cardiac beating rate to the anticancer drugs, Doxorubicin and Oxaliplatin, respectively. The beat rate represents the value after 48 h of drug exposure normalized by each tissue's beat rate at time 0, and then normalized by the value at 0 concentration. **(d, e)** The dose–response of the maximum capture rate of the cardiac tissues to Doxorubicin and Oxaliplatin, respectively, at the indicated concentration.

from a same parental iPS cell line to demonstrate the feasibility of creating patient-specific models. The iPS cells contain a GCaMP6-based fluorescent calcium reporter that, when combined with integrated gold electrodes, facilitates electrical pacing and assessment of cardiac function in real-time and noninvasively. We measured tumor growth and quantified the IC_{50} of the anticancer drugs, Doxorubicin and

Oxaliplatin. Doxorubicin reduced the spontaneous beating rate, maximum capture rate, and conduction velocity at or near the anticancer IC_{50}. In contrast, Oxaliplatin impacted similar indices of cardiac function only beyond the IC_{50}. These observations are consistent with the *in vivo* effects of Doxorubicin and Oxaliplatin. Our platform presents a unique system to examine the delivery of anticancer drugs
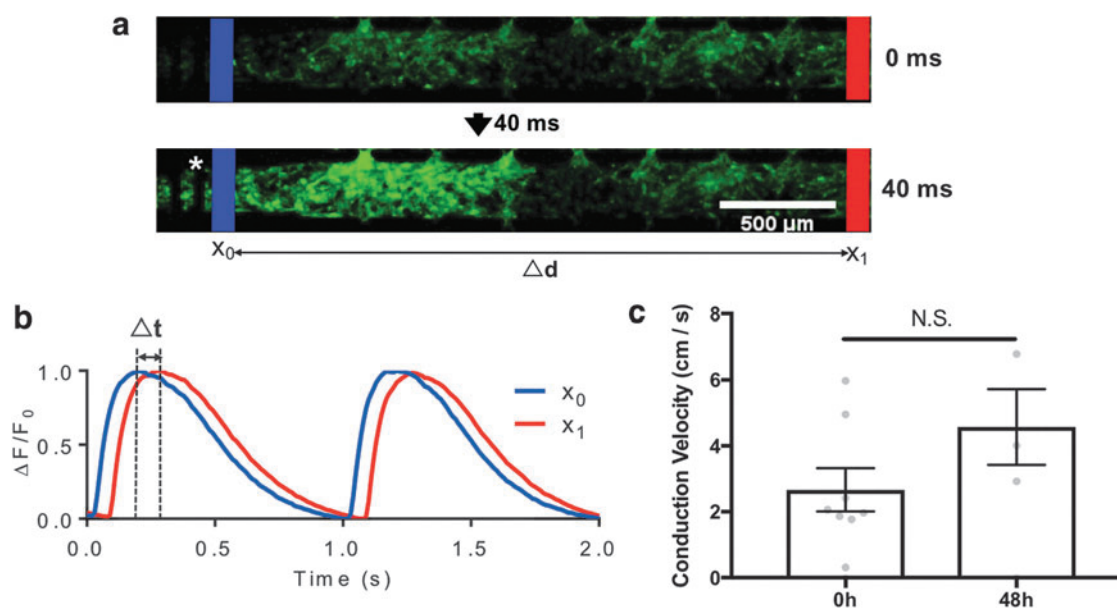
FIG. 5. Conduction velocity in cardiac tissues. **(a)** Fluorescence images of GCaMP6 at the indicated time. Two separated areas (x_0: *blue* and x_1: *red*) with known distance (Δd) were chosen from the image followed by the time (Δt) it took the fluorescent signal to traverse this distance. **(b)** The GCaMP6 intensities of each area. The time of peak of x_0 (*blue*) and x_1 (*red*) were determined using a custom-developed computer code and conduction velocity was determined as $\Delta d/\Delta t$. **(c)** The conduction velocity of cardiac tissues at 0 and 48 h. N.S. indicates not statistically significant.

across the endothelial barrier and assess the cytotoxicity of tumor cells and cardiac tissue simultaneously and may be a tool to improve the efficiency of the drug development process.

3D coculture of human cardiomyocytes, endothelial cells, and tumors

Many 3D models of human tumors,[17,18] iPS-CMs,[19,20] and iPS-ECs[14,21] have been presented and studied in the context of drug sensitivity and toxicity; however, our model is the first to culture all three systems on the same platform. The response of patients with cancer to chemotherapy is heterogeneous, and the creation of personalized predictive models using iPS technology could improve treatment outcomes. The coculture of three different cell types presents unique challenges, including choice of medium, volume of cells/tissues, and communication between the different tissues through convective and diffusive mass transport. We implemented a parallel design for the tissues that provides several advantages, including the loading of the tissues at flexible time points, and the delivery of drugs from the same vascular source (central chamber) ensuring the same concentration at the cardiac and tumor tissues. This design does not allow for the physiological recirculation of media, metabolism, or interaction between the organ systems that might occur *in vivo*, as has been previously demonstrated for multiple organ system mimics.[22–24] These potential disadvantages are not likely to be necessary for the cardiac tumor system as these organs do not ordinarily interact (e.g., tumors do not typically metastasize to the heart) *in vivo*.

Endothelial cell monolayer to mimic barrier properties

We and others have presented more complex 3D models of the human microcirculation, including the use of these sys-

tems to examine tumor drug sensitivity.[1,7,25] These systems generally involve the creation of 3D vascular networks that form through the process of vasculogenesis or angiogenesis and have the advantage of being dynamic and capable of responding (e.g., regressing or sprouting) to the drug of interest. However, these systems are also generally more complex, time consuming, and thus more expensive, to create. The surface area of vessels or capillaries (S) and associated volume of the tissue (V) that it serves is a major determinate of the activity of drug in the local tissue microenvironment. As such, we chose to design the microfluidic system to mimic a physiological V/S ratio. For this purpose, a simple monolayer of endothelial cells was sufficient to recapitulate the barrier function of the endothelial cell, and thus features of *in vivo* pharmacokinetics. Our data demonstrate that the iPS-EC monolayer provides a significant barrier to water and drug transport and was intact during the 48-h time window of the experiment. Nonetheless, perfused vascular networks may be more appropriate for studies that have a goal of examining drug effects on the microcirculation.

It is notable that the hydraulic conductivity (H_2O, molecular weight [MW] = 18 Da) of the cardiac tissue was similar to the tumor tissue (Fig. 2c), but the permeability of large molecules (Dextran, MW = 70 kD) through the cardiac tissue was higher than that of the tumor tissue (Fig. 2a, b). This difference is not likely to impact the drug testing response as the molecular weight of chemotherapeutic drugs is much smaller than 70 kD and the duration of the experiments spanned 48 h, which is much longer than the time required for both chambers to reach steady states (Supplementary Fig. S7). The transport of large molecules through the cardiac tissue is perhaps facilitated by mechanical strain of the endothelial monolayer (stretching of cell–cell junctional complexes) during contraction and relaxation. We also observed cytotoxicity of the endothelium layer in the

tissue chips that were treated with a high drug concentration. This could increase the permeability across the central chamber. However, an increased permeability would only reduce the time to reach a steady state (i.e., <80 min), and this time would remain much smaller than the time of drug exposure (48 h).

Simultaneous anticancer and cardiotoxicity testing

We chose to examine the effects of two drugs, Doxorubicin and Oxaliplatin, used clinically against colorectal carcinoma. Doxorubicin has well-documented cardiac toxicity,[26,27] and the precise mechanisms have been reported recently.[28–30] In contrast, Oxaliplatin has no documented cardiac toxicity. Our strategy was to determine the IC_{50} of the drugs toward tumor growth of a human colorectal cancer cell line, and then compare this dose–response to drug-induced cardiac toxicity. We purposely used simple (fluorescence) and rapid (instantaneous) readouts of cardiac toxicity that could be detected in less than 48 h. Our results demonstrate that Doxorubicin-induced cardiac toxicity occurs at or near the IC_{50} of the anticancer effect, whereas Oxaliplatin-induced cardiac toxicity occurred at concentrations significantly higher than the anticancer effect. This result is consistent with *in vivo* observations and suggests that, in principle, our relatively simple platform might be used to streamline the potential cardiac toxicity of anticancer drugs by examining these biological effects simultaneously.[31]

3D iPS-CMs to model cardiotoxicity

Several reports have demonstrated the utility of using both 2D and 3D models of iPS-derived human cardiomyocytes to examine drug toxicity.[24,32–34] Each of the proposed systems has distinct advantages, including simplicity and ease of use (2D monolayer) and physiological relevancy (3D mechanically conditioned). There has generally been a trade off—the more physiologically relevant the system, the longer the time and greater the resource required. As such, a model system should be chosen to reflect the physiological endpoints of interest. In our application, we wanted the cardiomyocytes to be in 3D, but we also wanted to minimize the time and resources required. We opted to load the iPS-CMs in a cell-dense solution to mimic the 3D nature of *in vivo* cardiomyocytes and began the drug exposure 48 h after cell loading. In an effort to minimize time and resources, we chose specifically not to condition the system mechanically or metabolically to mature the cells. Our data demonstrated that the iPS-derived cardiac tissue remained functional for 48 h in the integrated system; nonetheless, the 3D cardiomyocyte model was still able to replicate important *in vivo* features of cardiac toxicity.

Conclusion

In summary, we have developed a human tissue chip consisting of three organ systems (iPS-derived endothelium, iPS-derived 3D cardiomyocytes, and 3D tumor spheroids) in a simple parallel microfluidic design that facilitates the simultaneous examination of anticancer and cardiac toxicity of drugs. Compared with other multiorgan systems that employ complex tissue loading and plumbing, our design provides for simple loading of 3D tissues and the rapid (<48 h) assessment of anticancer and cardiotoxicity. The microtissues in the platform recapitulate important *in vivo* anticancer and cardiotoxicity effects of two well-known drugs—Doxorubicin and Oxaliplatin. Our platform could be used to improve the efficiency and thus lower the cost of preclinical drug discovery by simultaneously determining a drug's anticancer and cardiotoxicity potential.

Supplementary Material

Supplementary Figure S1
Supplementary Figure S2
Supplementary Figure S3
Supplementary Figure S4
Supplementary Figure S5
Supplementary Figure S6
Supplementary Figure S7
Supplementary Figure S8
Supplementary Figure S9

References

1. Phan, D.T.T., Wang, X., Craver, B.M., *et al.* A vascularized and perfused organ-on-a-chip platform for large-scale drug screening applications. Lab Chip **17,** 511, 2017.
2. Griffith, C.K., Miller, C., Sainson, R.C.A., *et al.* Diffusion Limits of an *in Vitro* Thick Prevascularized Tissue. Tissue Eng **11,** 257, 2005.
3. Burridge, P.W., Li, Y.F., Matsa, E., *et al.* Human induced pluripotent stem cell–derived cardiomyocytes recapitulate the predilection of breast cancer patients to doxorubicin-induced cardiotoxicity. Nat Med **22,** 547, 2016.
4. Hasinoff, B.B. The cardiotoxicity and myocyte damage caused by small molecule anticancer tyrosine kinase inhibitors is correlated with lack of target specificity. Toxicol Appl Pharmacol **244,** 190, 2010.
5. Morandi, P., Ruffini, P.A., Benvenuto, G.M., Raimondi, R., and Fosser, V. Cardiac toxicity of high-dose chemotherapy. Bone Marrow Transplant **35,** 323, 2005.
6. Shirure, V.S., Bi, Y., Curtis, M.B., *et al.* Tumor-on-a-chip platform to investigate progression and drug sensitivity in cell lines and patient-derived organoids. Lab Chip **18,** 3687, 2018.

7. Sobrino, A., Phan, D.T.T., Datta, R., *et al.* 3D microtumors in vitro supported by perfused vascular networks. Sci Rep **6,** 31589, 2016.

8. Jain, R.K., Martin, J.D., Chauhan, V.P., and Duda, D.G. Tumor microenvironment: vascular and extravascular compartment. In: Niederhuber, J.E., Armitage, J.O., Doroshow, J.H., Kastan, M.B., and Tepper, J.E., eds. Abeloff's Clinical Oncololy. Philadelphia, PA: Elsevier, Inc., 2020, pp. 108.

9. Rutkowski, J.M., and Swartz, M.A. A driving force for change: interstitial flow as a morphoregulator. Trends Cell Biol **17,** 44, 2007.

10. Shirure, V.S., Lezia, A., Tao, A., Alonzo, L.F., and George, S.C. Low levels of physiological interstitial flow eliminate morphogen gradients and guide angiogenesis. Angiogenesis **20,** 493, 2017.

11. Maddah, M., Heidmann, J.D.D., Mandegar, M.A.A., *et al.* A non-invasive platform for functional characterization of stem-cell-derived cardiomyocytes with applications in cardiotoxicity testing. Stem Cell Rep **4,** 621, 2015.

12. Lian, X., Hsiao, C., Wilson, G., *et al.* Robust cardiomyocyte differentiation from human pluripotent stem cells via temporal modulation of canonical Wnt signaling. Proc Natl Acad Sci U S A **109,** 1848, 2012.

13. Tohyama, S., Hattori, F., Sano, M., *et al.* Distinct metabolic flow enables large-scale purification of mouse and human pluripotent stem cell-derived cardiomyocytes. Cell Stem Cell **12,** 127, 2013.

14. Kurokawa, Y.K., Yin, R.T., Shang, M.R., Shirure, V.S., Moya, M.L., and George, S.C. Human induced pluripotent stem cell-derived endothelial cells for three-dimensional microphysiological systems. Tissue Eng Part C Methods **23,** 474, 2017.

15. Alonzo, L.F., Moya, M.L., Shirure, V.S., and George, S.C. Microfluidic device to control interstitial flow-mediated homotypic and heterotypic cellular communication. Lab Chip **15,** 3521, 2015.

16. Shirure, V.S., and George, S.C. Design considerations to minimize the impact of drug absorption in polymer-based organ-on-a-chip platforms. Lab Chip **17,** 681, 2017.

17. Zanoni, M., Piccinini, F., Arienti, C., *et al.* 3D tumor spheroid models for in vitro therapeutic screening: a systematic approach to enhance the biological relevance of data obtained. Sci Rep **6,** 19103, 2016.

18. Aw Yong, K.M., Li, Z., Merajver, S.D., and Fu, J. Tracking the tumor invasion front using long-term fluidic tumoroid culture. Sci Rep **7,** 10784, 2017.

19. Mathur, A., Loskill, P., Shao, K., *et al.* Human iPSC-based cardiac microphysiological system for drug screening applications. Sci Rep **5,** 8883, 2015.

20. Huebsch, N., Loskill, P., Deveshwar, N., *et al.* Miniaturized iPS-cell-derived cardiac muscles for physiologically relevant drug response analyses. Sci Rep **6,** 24726, 2016.

21. Ohtani-Kaneko, R., Sato, K., Tsutiya, A., Nakagawa, Y., Hashizume, K., and Tazawa, H. Characterisation of human induced pluripotent stem cell-derived endothelial cells under shear stress using an easy-to-use microfluidic cell culture system. Biomed Microdevices **19,** 91, 2017.

22. Skardal, A., Murphy, S.V., Devarasetty, M., *et al.* Multitissue interactions in an integrated three-tissue organ-on-a-chip platform. Sci Rep **7,** 8837, 2017.

23. Edington, C.D., Chen, W.L.K., Geishecker, E., *et al.* Interconnected microphysiological systems for quantitative biology and pharmacology studies. Sci Rep **8,** 4530, 2018.

24. Oleaga, C., Bernabini, C., Smith, A.S.T., *et al.* Multi-Organ toxicity demonstration in a functional human in vitro system composed of four organs. Sci Rep **6,** 20030, 2016.

25. Heylman, C., Sobrino, A., Shirure, V.S., Hughes, C.C.W., and George, S.C. A strategy for integrating essential three-dimensional microphysiological systems of human organs for realistic anticancer drug screening. Exp Biol Med **239,** 1240, 2014.

26. Lefrak, E.A., Pitha, J., Rosenheim, S., and Gottlieb, J.A. A clinicopathologic analysis of adriamycin cardiotoxicity. Cancer **32,** 302, 1973.

27. Von Hoff, D.D., Layard, M.W., Basa, P., *et al.* Risk factors for doxorubicin-induced congestive heart failure. Ann Intern Med **91,** 710, 1979.

28. Deavall, D.G., Martin, E.A., Horner, J.M., and Roberts, R. Drug-induced oxidative stress and toxicity. J Toxicol **2012,** 13, 2012.

29. Zhang, S., Liu, X., Bawa-Khalfe, T., *et al.* Identification of the molecular basis of doxorubicin-induced cardiotoxicity. Nat Med **18,** 1639, 2012.

30. Hanna, A.D., Lam, A., Tham, S., Dulhunty, A.F., and Beard, N.A. Adverse effects of doxorubicin and its metabolic product on cardiac RyR2 and SERCA2A. Mol Pharmacol **86,** 438, 2014.

31. Beaumont, P.O., Moore, M.J., Ahmad, K., Payne, M.M., Lee, C., and Riddick, D.S. Role of glutathione S-transferases in the resistance of human colon cancer cell lines to doxorubicin. Cancer Res **58,** 947, 1998.

32. McCain, M.L., Sheehy, S.P., Grosberg, A., Goss, J.A., and Parker, K.K. Recapitulating maladaptive, multiscale remodeling of failing myocardium on a chip. Proc Natl Acad Sci U S A **110,** 9770, 2013.

33. Huebsch, N., Loskill, P., Mandegar, M.A., *et al.* Automated video-based analysis of contractility and calcium flux in human-induced pluripotent stem cell-derived cardiomyocytes cultured over different spatial scales. Tissue Eng Part C Methods **21,** 467, 2015.

34. Nunes, S.S., Miklas, J.W., Liu, J., *et al.* Biowire: a platform for maturation of human pluripotent stem cell-derived cardiomyocytes. Nat Methods **10,** 781, 2013.

Address correspondence to:
Steven C. George, MD, PhD
Department of Biomedical Engineering
University of California, Davis
451 East Health Sciences Drive, GBSF
Room 2303
Davis, CA 95616

E-mail: scgeorge@ucdavis.edu